FERMILAB-PUB-20-268-TD
ACCEPTED

Persistent compositions of non-stoichiometric compounds with low bulk diffusivity: a theory and application to Nb_3Sn superconductors

X. Xu [a, *], M.D. Sumption [b], J. Lee [c], J. Rochester [b], X. Peng [d]

[a] *Fermi National Accelerator Laboratory, Batavia, IL 60510, USA*

[b] *Department of Materials Science and Engineering, the Ohio State University, Columbus, OH 43210, USA*

[c] *Department of Materials Science and Engineering, Northwestern University, Evanston, IL 60208, USA*

[d] *Hyper Tech Research Incorporated, 539 Industrial Mile Road, Columbus, OH 43228, USA*

* Corresponding author. *E-mail address: xxu@fnal.gov*

Abstract

Non-stoichiometric compounds may develop a composition gradient when they are formed by reactive diffusional processes. This paper reports an interesting phenomenon that in compounds with low bulk diffusivities, which rely mainly on grain boundary diffusion for their growth, the final bulk compositions may be far from equilibrium, with a very low bulk diffusivity leading to fixed (persistent) compositions – one such example is Nb_3Sn, a superconductor. We investigated the microchemistry at the reactive interface using atom probe tomography to clarify the diffusion reaction mechanism for this low-bulk-diffusivity case and thus propose a theory for what determines the compound composition, using Nb_3Sn as an example for concreteness. Using certain approximations, we derive an explicit analytical equation that illustrates what factors determine its composition profile. We compare our model with the known facts of Nb_3Sn and see good agreement. In particular, this model predicts that internal oxidation may lead to higher Sn contents than conventional, non-oxidized Nb_3Sn. Our measurements show that this is indeed true, and that the internally-oxidized Nb_3Sn also has higher upper critical fields, achieving up to 28.2 T at 4.2 K. We discuss the general applicability of this model to non-stoichiometric compounds with low bulk diffusivity, and propose it as a tool to help in the design and processing of such materials for compositional control.

Keywords: Non-stoichiometric compounds, Compositions, Grain boundary diffusion, Solid state reactions, Nb_3Sn superconductor, Internal oxidation

1. Introduction

Non-stoichiometric compounds (i.e., those with stoichiometric ratios that can vary in finite ranges) represent a large class of materials. In many of these materials their compositions have significant influence on their performance for relevant applications. This performance can be related to their mechanical properties (e.g., Ni-$Al_{0.4\text{-}0.55}$ [1]), superconducting properties (e.g., $NbB_{2\text{-}2.8}$ [2]), or catalytic properties (e.g., Zn-$Pd_{46.8\text{-}59.1}$ [3]), to give a few examples. In many cases such compounds are products of diffusional reactions, where the formed compound has certain layer thickness through which the diffusing species must travel to reach the reaction

front. This typically leads to a composition gradient in the compound layer, with the compositions at all points falling somewhere within the composition range given by the equilibrium phase diagram because limited reaction rates at interfaces lead to discontinuity in the chemical potential across the interfaces.

One example of that is given by the case of Nb_3Sn, an A15-structure intermetallic compound with a Sn content range of around 17-25.5 at.% [4,5]. In practical terms it is a technical superconductor for fabricating high-field superconducting magnets above ~10 T, and has found a series of important applications [5]. Research and development of Nb_3Sn materials are regaining significant interest worldwide in recent years because they are the conductors of choice to build accelerator magnets for the planned Future Circular Collider (FCC); however, the performance of the state-of-the-art Nb_3Sn is significantly below that required by FCC specification [6], motivating researchers to explore further improvement. For Nb_3Sn, the Sn content is a primary factor determining its critical temperature (T_c) and upper critical field B_{c2}, with lower Sn content leading to significantly poorer T_c and B_{c2} [5,7-8]. In a Nb_3Sn superconductor a Nb_3Sn layer is formed in a Sn/Nb diffusion reaction process and this layer contains a Sn content range, which has significant influence on its performance: e.g., a recent modeling study by Baumgartner et al. showed that improving the Sn content and reducing its gradient in the Nb_3Sn layer could be a potential way to approach the FCC specification [9]. However, even though improving the Sn content has been a critical goal for Nb_3Sn conductor development since its composition–performance correlation was discovered in the early 1980s [7,8], and observations of experimental results in the past few decades have led to a few semi-empirical conclusions (e.g., high-Sn Cu-Sn as Sn source tends to form Nb_3Sn with higher Sn content [10]), a clear, systematic understanding of what determines the Sn content profile of a Nb_3Sn layer, as it forms from the Sn/Nb diffusion reaction process, has not been obtained so far, let alone a quantitative, explicit treatment with predictive power.

But Nb_3Sn is only one of the non-stoichiometric compounds for which a clear understanding of what determines their compositions is very desirable (due to the influence of compositions on their properties). However, while a lot of previous studies on diffusion reaction systems were focused on subjects such as layer growth kinetics and compound presence (e.g., [11]), etc., to the best of our knowledge there has been no systematic theory illustrating what determines compositions of non-stoichiometric compounds formed in diffusion reaction processes. This is not very surprising because in a common diffusion reaction model the compound composition is not constant, but changes with annealing time (e.g., as the layer grows or as the chemical potential profile of the system evolves). However, during our studies of Nb_3Sn, we found an interesting fact that the composition profile of a formed Nb_3Sn layer had little change with annealing time. We correlated this to the very low bulk diffusivity in Nb_3Sn, which leads to bulk compositions that are far from equilibrium (elaborated below). Thus, the above-mentioned changing composition in a common diffusion reaction model is in fact based on an automatic assumption of considerable bulk diffusion, which of course allows the bulk composition of a formed compound layer to change. On the other hand, when we come to the case of a compound with low bulk diffusivity (e.g., Nb_3Sn) that makes its bulk compositions persistent (or nearly-persistent), a understanding of what determines its compositions now becomes much more useful. This paper aims to fill this gap. To do so, we will, for concreteness and clarity, choose Nb_3Sn as a specific example, and describe our theory

for that particular case. This is a particularly useful example because (i) much data is extant on Nb_3Sn for model validation, and (ii) the composition of Nb_3Sn is critical for its performance, which is very motivating, as discussed previously. We have performed some exploration of this general area of inquiry [10,12], but were ultimately limited by a lack of knowledge of some microchemistry details that are needed to understand the diffusion reaction mechanism in the case of low bulk diffusivity. This is now present, available based on chemical analyses particular on the reactive interface. Using this information, we are able to more fully and predictively describe the diffusion reaction process in this paper, and using some approximations we derive an explicit analytical equation for the composition profile showing the determining factors. We then compare the model to the known facts of Nb_3Sn for validation. We also use this model to predict the compositions of an emerging new-type Nb_3Sn, which is based on the internal oxidation technology [13]. This technology introduces O and Zr (or alternatively Ti, Hf, Al) separately to Nb_3Sn precursors so that during heat treatment, while a Nb_3Sn layer forms in the diffusion reaction system, O selectively oxidizes Zr (or Ti, Hf, Al) to form ZrO_2 (or TiO_2, HfO_2, Al_2O_3) nanoparticles in Nb_3Sn. This new type of Nb_3Sn has demonstrated superior performance to conventional Nb_3Sn [13,14]. In particular, we found that internal oxidation of Nb_3Sn influences certain parameters in our equation, which provides an ideal opportunity to validate the soundness of this model. In the end we briefly discuss the possibility of using our theory generally for other non-stoichiometric compounds with low bulk diffusivity.

2. Theory and validation

As mentioned above, we found that the bulk diffusivity has a critical influence on the composition of a non-stoichiometric compound formed in a diffusion reaction process, with a low bulk diffusivity leading to interesting features quite distinct from those in a compound with high bulk diffusivity. In order to show these features specifically, let us use Nb_3Sn as an example. Below is a brief introduction to the Nb_3Sn system that is relevant for the discussion. Fig. 1a shows the Nb-Sn phase diagram below 800°C [4] (the temperatures to use for Sn+Nb reaction to form Nb_3Sn are typically between 600-800°C, mostly 625-700°C for practical applications). Reaction of elemental Sn and Nb below 800°C would form first $NbSn_2$, which would then transform to Nb_6Sn_5 and finally to Nb_3Sn (assuming Nb in excess). A technologically useful Nb_3Sn superconductor is normally in the form of a wire, which is comprised of a number of Nb_3Sn filaments (and a few Cu filaments) embedded in a Cu matrix. As an illustration, scanning electron microscopy (SEM) images of an internal oxidation wire with 180/217-filament design (i.e., 180 Nb_3Sn and 37 Cu filaments) after heat treatment (685°C/120h) are shown in Figs. 1b and 1c. More details of this wire will be given in Section 3. Each Nb_3Sn filament is an independent diffusion-reaction unit (separated from the outside Cu matrix by a barrier), which, in the as-fabricated state, is typically composed of a Sn-source (usually Cu+Sn) core surrounded by a Nb alloy tube (or variant). These precursors require a heat treatment for the formation of the Nb_3Sn phase. Cu is added into the Sn source core in each Nb_3Sn filament because Cu can promote the formation rate of Nb_3Sn by destabilizing $NbSn_2$ and Nb_6Sn_5 [15], but Cu has low solubility in Nb_3Sn lattice [16]. It was found that if the Sn/Cu atomic ratio is above 1/3, Nb_6Sn_5 will form, which initially serves as a Sn source for the

Nb_3Sn formation until it is consumed, after which the low-Sn Cu-Sn alloys (with Sn content below 25at.%) take over [10]; the Sn content in the Cu-Sn alloys drops as its Sn is consumed for Nb_3Sn layer growth until the Sn source is depleted (or the heat is removed). In the Sn-source/Nb_3Sn/Nb diffusion reaction system (a schematic of this system and its Sn content profile is shown in Fig. 1d), Sn is the diffusing species in Nb_3Sn (as judged by the location of Kirkendall voids [10]): during heat treatment Sn diffuses out from the Sn source, across the growing Nb_3Sn layer, to the Nb_3Sn/Nb interface where the reaction front of the Nb+Sn → Nb_3Sn reaction is located.

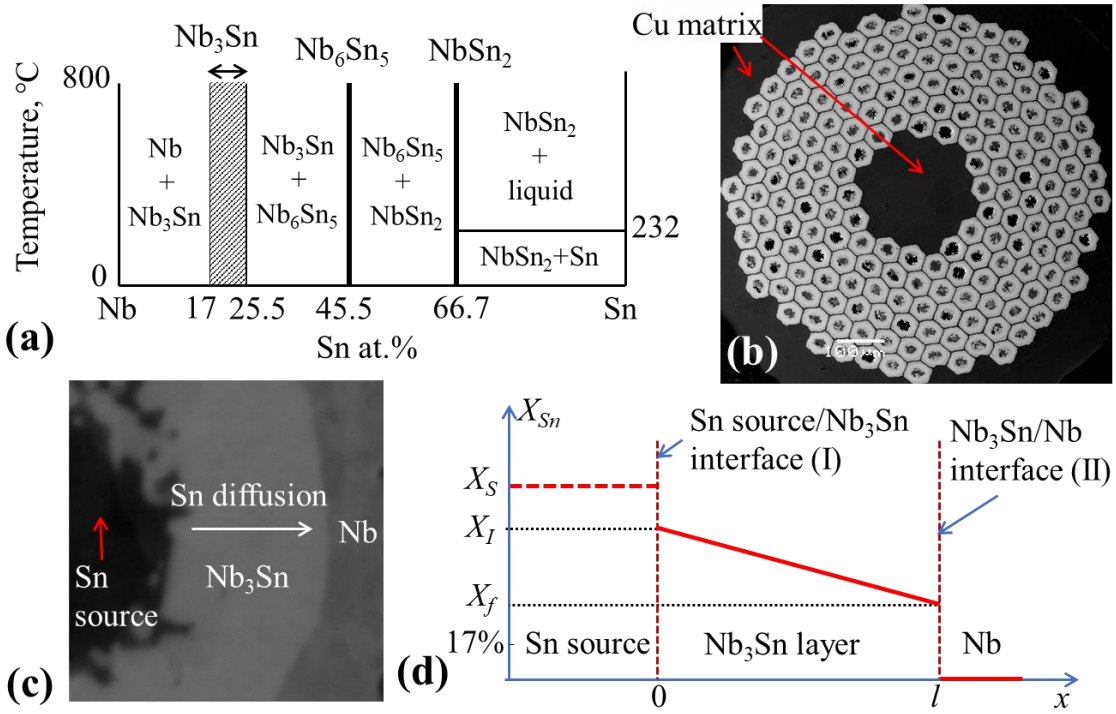

Fig. 1. (a) Binary Nb-Sn phase diagram below 800°C (after [4]), (b) SEM image of an internal-oxidation-type wire after 685°C/120h heat treatment, (c) zoom-in of a filament to show the Sn-source/Nb_3Sn/Nb diffusion reaction system, (d) a schematic of the Sn-source/Nb_3Sn/Nb diffusion reaction system with the Sn content profile. The parameters X_s, X_I, and X_f are to be explained later.

Let us first assume that Nb_3Sn has a high bulk diffusivity and see if this agrees with facts. With a high bulk diffusivity, when the Sn source is a Cu-Sn alloy, as the Sn content in Cu-Sn drops with the Nb_3Sn layer growth, the Sn content level of the Nb_3Sn layer is expected to drop accordingly because the chemical potential of Sn (μ_{Sn}) in the Sn source must be higher than the μ_{Sn} of Nb_3Sn. If Nb is in excess, with sufficiently long annealing time, the Sn source will eventually be "depleted" when its μ_{Sn} drops to a level such that the Sn source reaches equilibrium with the unreacted Nb – in fact, in this case the Sn source, the Nb_3Sn layer, and the unreacted Nb are all in equilibrium, which, based on the Nb-Sn phase diagram (Fig. 1a), means the Nb_3Sn layer should have a uniform composition of Nb-17at.%Sn. In reality, pushing Nb_3Sn wires to full reaction is quite typical, and our measurements show that the Sn content in the remaining Cu-Sn core after depletion is usually only 0.2-1.0 at.% (depending on reaction

temperature), but contrary to the above predictions about Nb_3Sn composition based on high bulk diffusivity, the Nb_3Sn layer composition has never been found to be Nb-17%Sn after Sn source depletion. Furthermore, we measured the change of the Sn content profile of a Nb_3Sn layer as the Sn content of the Cu-Sn source was decreasing, and found that it kept more or less persistent [12]. In fact, we found that even after extended annealing after the Sn source was depleted, the Nb_3Sn layer composition still had little change. For example, we reacted wires with small filament sizes at 800°C for 1 hour (the Sn source was already depleted at this time), which generated Nb_3Sn layers with Sn content profiles between 22.5-24.5 at.% [17]; then we extended the annealing time to 100 hours. If the bulk diffusivity was high, we would expect the Nb_3Sn layers to transform towards Nb-17%Sn (in order to reach equilibrium with the unreacted Nb), with the released Sn reacting with Nb to form thicker Nb-17%Sn layers. However, in reality we observed that the extremely long annealing time led to little Sn content drop or further Nb_3Sn layer thickness growth [17]. In fact, we also noticed in a previous study [18] that the superconducting properties had little change when the annealing time at 750°C was extended from 8 hours (long enough to deplete the Sn source) to 110 hours; based on the correlation between Nb_3Sn superconducting properties and its Sn content [5,18], this result actually also indicated the persistent behavior of Nb_3Sn composition.

We ascribe this extraordinary phenomenon of persistent composition to a very low bulk diffusivity in Nb_3Sn. The exact values of bulk diffusivity of Sn in Nb_3Sn have not been reported, but were suggested in [19] to be below 10^{-23} m^2/s at 800°C, which, based on the relation that the diffusion distance roughly equals to square root of the product of diffusivity and time, leads to a bulk diffusion distance of <2 nm for 100 hours at 800°C. Of course, the bulk diffusivity at a practical heat treatment temperature for Nb_3Sn wires in real applications (typically at 625-700°C, while a temperature above 700°C is very rare for modern Nb_3Sn conductors in practical use) can only be even much lower. On the other hand, the diffusivity of Sn along Nb_3Sn grain boundaries is over 9 orders of magnitude higher than that of the bulk diffusivity [19], which, combined with the small Nb_3Sn grain size (typically 60-200 nm), dictates that Sn diffuses mainly through the Nb_3Sn layers along the grain boundaries.

However, one important question is, if Sn cannot readily diffuse in Nb_3Sn lattice and thus only effectively diffuses along the Nb_3Sn grain boundaries, how can the Sn+Nb reaction be sustained at the Nb_3Sn/Nb interface? It is impossible to answer this question without a better knowledge of the Nb_3Sn/Nb interface. Thus, we have employed atom probe tomography (APT) to directly explore the Nb_3Sn/Nb interface; we chose here to look at a high-performance internal-oxidation-type Nb_3Sn wire (with Zr and O added). Fig. 2a shows a 3-D reconstruction of an APT nanotip containing a Nb_3Sn/Nb interface, Fig. 2b displays distributions of Nb and Sn elements in a cross section of the APT nanotip shown in Fig. 2a, Fig. 2c displays distributions of Cu and Zr-O ions, and Fig. 2d shows concentrations of Cu, Zr, and O across the Nb_3Sn/Nb interface.

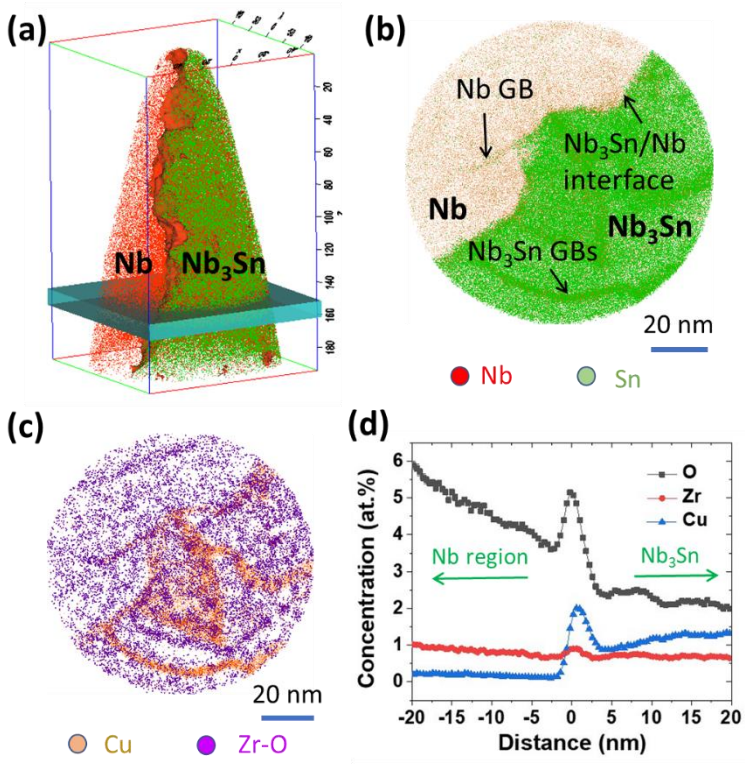

Fig. 2. (a) 3-D reconstruction of an APT nanotip containing a Nb_3Sn/Nb interface, (b) distributions of Nb and Sn atoms in a cross section of the APT nanotip shown in Fig. 2a, (c) distributions of Cu and Zr-O ions, (d) concentrations of Cu, Zr, and O across the Nb_3Sn/Nb interface.

It has been reported that Cu segregates at Nb_3Sn grain boundaries while having low solubility in Nb_3Sn lattice [16], which can also be seen in Fig. 2c. Furthermore, from Fig. 2c we can see that there is also a high concentration of Cu at the Nb_3Sn/Nb interface, similar to that at Nb_3Sn grain boundaries. The composition scan across the interface in Fig. 2d shows quantitatively the concentrations of some elements, from which we can not only verify the high concentration of Cu, but also see large amounts of Zr and O at the Nb_3Sn/Nb interface. It is worth noting that our APT results (Figs. 2c and 2d) show that the width of the region with high impurity concentrations at the interface is similar to that at Nb_3Sn grain boundaries (a concentration profile across a Nb_3Sn grain boundary we obtained using the same APT technique can be found in [20]), indicating that the Nb_3Sn/Nb interface may have a similar characteristic to Nb_3Sn grain boundaries with respect to being diffusion paths for Cu and Sn. This could be because the vacancies in the interface and the grain boundaries, which can accommodate high concentrations of impurities with relatively low energy penalty, also allow atoms to diffuse relatively fast along these disordered structures. Therefore, a possible mechanism for the diffusion process in the case of low bulk diffusivity is that Sn atoms first diffuse along Nb_3Sn grain boundaries, reach the intersections of the Nb_3Sn grain boundaries and the Nb_3Sn/Nb interface, and then diffuse at the interface from these intersections. Furthermore, based on our studies we do not see any Sn concentration gradient at the Nb_3Sn/Nb interface, indicating that the Sn transport rate at the interface must be higher than that along

the Nb_3Sn grain boundaries – this is perhaps because the maximum Sn diffusion distance at the interface is only tens of nanometers (which is half of the geometric distances between the intersections of the interface and the Nb_3Sn grain boundaries) while the Sn diffusion distance along Nb_3Sn grain boundaries is mostly micrometers (from the Sn source to the Nb_3Sn/Nb interface). Therefore, for the analysis below we assume the diffusion along Nb_3Sn grain boundaries is the limiting process for the whole Sn diffusion process that supplies Sn for new Nb_3Sn formation.

Based on the above picture of the diffusion mechanism, we propose our theory for the bulk composition in the case of low bulk diffusivity as below. As new atomic layers of Nb_3Sn form and the Nb_3Sn/Nb interface moves ahead, the Nb_3Sn atomic layers that were previously in the diffusion zone at the Nb_3Sn/Nb interface are now left behind in the newly formed "bulk"; then due to the extremely low bulk diffusivity, the Sn vacancies in these now bulk atomic layers are frozen inside the lattice (or transform to Nb-on-Sn antisites): i.e., the Sn contents of these layers are now fixed and cannot change, regardless of the μ_{Sn} change in the system. This explains the experimental results mentioned previously that the Sn contents changed hardly at all even after extremely long annealing times. From this picture we see that the resultant bulk Sn content profile of a final Nb_3Sn layer is in fact an accumulation of local "snapshots" of the Sn contents of the "frontier" Nb_3Sn layers (i.e., the atomic layers in the diffusion zone at the Nb_3Sn/Nb interface) just before they break away from the diffusion zone at the interface. If we denote the Sn content of a "frontier" layer as X_f, then the bulk Sn content profile of a final Nb_3Sn layer is simply an accumulation of X_f at each layer thickness.

So, what determines the Sn content of a frontier Nb_3Sn layer? Below is a qualitative analysis. Based on the Nb-Sn phase diagram, as long as X_f is higher than 17 at.%, the frontier layer tends to transform to Nb-17%Sn to reach equilibrium with Nb (this can happen because this frontier layer is in the diffusion zone at the Nb_3Sn/Nb interface), with the released Sn reacting with Nb to form new Nb_3Sn (also Nb-17%Sn). On the other hand, if the frontier layer in fact has a composition of Nb-17%Sn, its μ_{Sn} would be lower than that of the Sn source (if not yet depleted); this μ_{Sn} difference is a driving force for Sn to diffuse to the frontier layer to enhance its Sn content (again, this can happen because the frontier layer is connected to the diffusion path). From these discussions we see that there are two competing processes that determine X_f: (1) the transfer of Sn from the frontier layer to the Nb region to form new Nb_3Sn (i.e., the reaction process at the Nb_3Sn/Nb interface), which tends to reduce X_f towards 17%, (2) the diffusion process that transports Sn from the Sn source to the frontier layer, which tends to enhance X_f towards some value that makes its μ_{Sn} equal to that of the Nb_3Sn grain boundaries next to the Sn source. If the diffusion rate is slow relative to the reaction rate at the Nb_3Sn/Nb interface, the Sn supply is only sufficient to maintain the growth of a Nb_3Sn layer with a lower Sn content. If, on the other hand, the reaction rate at the Nb_3Sn/Nb interface is slow relative to the diffusion rate, the frontier layer cannot develop as large a μ_{Sn} difference with the Nb_3Sn grain boundaries next to the Sn source – in this case, X_f would increase until a balance is reached between these two processes; of course its maximum is limited by the μ_{Sn} of the Sn source and the reaction rate (i.e., the Sn transfer rate) at the Sn source/Nb_3Sn interface because a μ_{Sn} discontinuity across this interface may exist depending on the reaction rate at this interface (a lower reaction rate leads to a larger μ_{Sn} discontinuity). From this qualitative analysis, we see that there are four factors determining X_f: a higher reaction rate at the Nb_3Sn/Nb interface tends

to reduce X_f, while a higher diffusion rate, a higher μ_{Sn} of the Sn source, and a higher reaction rate at the Sn source/Nb_3Sn interface tend to enhance X_f.

The above qualitative analysis provides a preliminary understanding of what determines X_f, but we still need a quantitative model. In order to obtain a simple analytical solution that can directly show all the factors and how they influence the composition, let us make some reasonable simplifications and consider the case in one dimension. A schematic of the concentration profile for this diffusion reaction system is shown in Fig. 1d. Because Sn diffuses along Nb_3Sn grain boundaries, only a fraction of the cross-sectional area perpendicular to the diffusion direction is effective as a diffusion channel, and this fraction can be estimated as $1-d^2/(d+w)^2 \approx 2w/d$ (since $w << d$), where w (in nm) is the width of Nb_3Sn grain boundaries in which Sn diffuses and d (in nm) is the average grain size. Assuming a steady-state diffusion, with the mole fraction of Sn in the Nb_3Sn grain boundaries next to the Sn source denoted X_I, the Sn diffusion flux (in mol/m^2-s) to the frontier layer is given by: $J_d = D/V_m \cdot (2w/d) \cdot (X_I - X_f)/l$, in which D (in m^2/s) is the Sn diffusivity along Nb_3Sn grain boundaries, V_m is the molar volume of Nb_3Sn (~44.6 cm^3/mol), and l (in m) is the Nb_3Sn layer thickness (i.e., the distance of the frontier layer from the Sn source, see Fig. 1d). If we define an effective diffusivity $D_{eff} = D/V_m \cdot (2w/d)$, which has a unit of mol/m-s, J_d can be written in a simple form:

$$J_d = D_{eff} \cdot (X_I - X_f)/l \tag{1}$$

Next, let us consider the reaction rates at the interfaces (expressed in terms of the Sn fluxes across the interfaces). As shown in Fig. 1d, let us denote the Sn source/Nb_3Sn interface as Interface I and the Nb_3Sn/Nb interface as Interface II. The μ_{Sn} discontinuity across an interface is the driving force for transfer of Sn atoms and, together with a pre-factor, determines the reaction rate at this interface. A derivation of the reaction rate at an interface is shown in the Appendix, using the Nb_3Sn/Nb interface as the example, which gives that the reaction rate at the Interface II is:

$$J_{II} = k_{II}(X_f - 17\%) \tag{2}$$

where k_{II} is the reaction rate constant (in mol/m^2-s) for Interface II. We can use a similar treatment for Interface I; however, we need to first define an imaginary Sn content X_s for the Sn source that makes the μ_{Sn}(Sn source) equal to μ_{Sn}(Nb-X_sSn). Note that X_s is not the real Sn content in the Sn source, but an equivalent Sn content in Nb_3Sn such that this Nb_3Sn has the same μ_{Sn} with the Sn source. For example, if the Sn source is Nb_6Sn_5, then X_s = 25.5% because μ_{Sn}(Nb-25.5%Sn) = μ_{Sn}(Nb_6Sn_5). If the Sn source is a Cu-Sn alloy, X_s depends on the Sn content in the Cu-Sn – while the relation is not so explicit, a possible relation was proposed in [12]. Using the parameter X_s, we can express the reaction rate at the Interface I as:

$$J_I = k_I(X_s - X_I) \tag{3}$$

where k_I is the reaction rate constant (in mol/m^2-s) for the Interface I. According to mass conservation, J_d, J_I, and J_{II} must be equal, so by solving the equation set of Eqs. (1) - (3), we can obtain X_f:

$$X_f = 17\% + \frac{X_S - 17\%}{1 + k_{II}/k_I + (k_{II}/D_{eff})\cdot l} \quad (4)$$

This equation expresses X_f with l, with three parameters that depend on each specific system: X_s, k_{II}/k_I, and k_{II}/D_{eff}. As mentioned earlier, the composition profile of a growing Nb_3Sn layer is an accumulation of each X_f at each layer thickness; thus, Eq. (4) in fact shows the Sn content profile in a formed Nb_3Sn layer (with l treated as the variable: i.e., the distance from the Sn source) – but one thing that must be pointed out is that X_s may not be a constant when Cu-Sn alloys serve as the Sn source (because X_s drops as l increases). However, if the Sn source is Nb_6Sn_5, X_s is constant (25.5%); then it is possible to use Eq. (4) to fit a Sn content profile of a Nb_3Sn layer in order to obtain the k_{II}/k_I and k_{II}/D_{eff} parameters. An example is given in Fig. 3a, where the data of a so-called "tube type" wire [10,21] (a wire type without internal oxidation) from a previous study (the 650°C/48h sample in [21]) are used, for which the Sn source was only Nb_6Sn_5. It can be seen that the fitting is reasonably good, and the obtained k_{II}/k_I is 0.233, and the k_{II}/D_{eff} is 0.11/m. In Figs. 3b, 3c, and 3d we show the Sn content profiles calculated from Eq. (4) for varying the k_{II}/k_I, k_{II}/D_{eff}, and X_s in turn, in order to see how each factor influences the X_{Sn} profiles. In Fig. 3b we keep X_s = 25.5% and k_{II}/D_{eff} = 0.1/m, and plot the Sn content profiles for k_{II}/k_I = 0.01, 0.1, 1, 10, and 100. In Fig. 3c we keep X_s = 25.5% and k_{II}/k_I = 0.1, and plot X_{Sn} profiles for k_{II}/D_{eff} = 0.01/m, 0.1/m, 1/m, 10/m, and 100/m. In Fig. 3d we keep k_{II}/k_I = 0.1 and k_{II}/D_{eff} = 0.01/m, and plot $X_{Sn}(l)$ for four cases: X_s = 25.5%, X_s dropping from 25.5% by 0.5% as the Nb_3Sn layer grows by 1 μm, X_s dropping from 25.5% by 1% as the Nb_3Sn layer grows by 1 μm, and X_s = 17%. One thing that must be pointed out is that the curves displayed in Fig. 3 do not represent all the possible Sn content profile shapes in Nb_3Sn wires. This is because in real wires the change of X_s with l can be complicated and thus generate different profiles. One example is given here: a common case for modern Nb_3Sn wires is that, Nb_6Sn_5 first serves as the Sn source (making X_s = 25.5%) before Cu-Sn alloys take over, and the Sn content drop in the Cu-Sn causes a X_s drop, but this X_s drop with Sn content decrease in Cu-Sn is not linear; instead, X_s drops faster as the Sn content in the Cu-Sn is lower [12]. In such a case, the Sn content profile would have a concave-down shape.

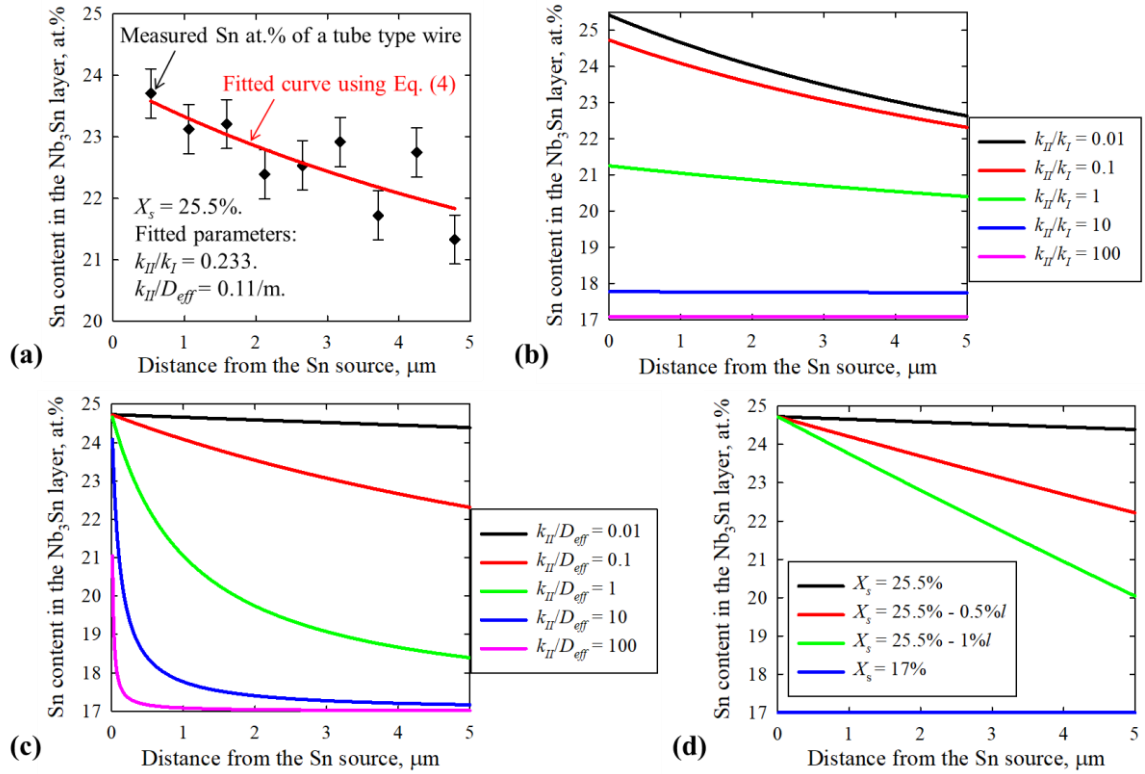

Fig. 3. (a) Fitting of the Sn content profile of a "tube type" Nb_3Sn wire (a wire type without internal oxidation) with only Nb_6Sn_5 as the Sn source [21] using Eq. (4), and plots of the calculated Sn content profiles for (b) varying k_{II}/k_I while keeping X_s = 25.5% and k_{II}/D_{eff} = 0.1/m, (c) varying k_{II}/D_{eff} while keeping X_s = 25.5% and k_{II}/k_I = 0.1, (d) varying X_s while keeping k_{II}/k_I = 0.1 and k_{II}/D_{eff} = 0.01/m.

It can be seen from Figs. 3b, 3c, and 3d that each of these factors has a significant influence on the Sn content profile. Let us analyze how they each influence the Sn content of Nb_3Sn, and also compare the predictions of this theory to the known facts gleaned from the experimental observations of many groups over the past few decades.

- ***X_s*:** clearly lower X_s leads to lower Sn content. In reality the Sn source was indeed found to have a significant impact on the Sn content of Nb_3Sn; comparison of Nb_3Sn wires with different Sn sources clearly indicates that Sn sources with higher μ_{Sn} tend to form Nb_3Sn with higher Sn contents and lower Sn content gradients [10]. In fact, X_s has a dramatic influence on the Sn content gradient of a Nb_3Sn layer due to decrease in X_s with l when low-Sn Cu-Sn alloys serve as the Sn source. This can be most clearly seen in "bronze-process" Nb_3Sn wires which use bronze as the Sn source: the Sn content is relatively high for the initial Nb_3Sn layers (i.e., those formed first, when l is small), but drops quickly as the diffusion distance increases [22].
- ***k_{II}/k_I*:** this parameter has a dramatic influence on the composition at l = 0, with larger k_{II}/k_I leading to decrease in the Sn content. The importance of this parameter has not been revealed by previous experiments, but its influence can be easily understood: a larger reaction rate constant at an interface leads to a smaller chemical potential discontinuity across the interface. Thus, larger k_{II} means that X_f is closer to 17%, while larger k_I means X_I is closer to X_s. Clearly, a larger k_I and a smaller k_{II} are beneficial to the Sn content in

the Nb_3Sn layer.

- ***k_{II}/D_{eff}*:** this parameter, which in fact reflects the competition between the diffusion rate and the reaction rate at the Nb_3Sn/Nb interface mentioned in our qualitative analysis earlier, has a direct influence on the Sn content gradient, with a larger k_{II}/D_{eff} leading to a larger Sn content gradient, which agrees with our qualitative analysis before. Since $D_{eff} = D/V_m \cdot (2w/d)$, smaller reaction rate constant k_{II}, smaller grain size d, larger grain boundary width w, and larger grain boundary diffusivity D (which, taken together mean lower reaction rate and higher diffusion rate) tend to reduce the Sn content gradient of Nb_3Sn. The influence of reaction rate versus diffusion rate has not been noted before; however, in this paper we show that this plays a key role, especially in the new internally-oxidized Nb_3Sn.

We see that the model agrees well with the above qualitative analysis and the known facts of Nb_3Sn composition, although these known facts only represent the tip of the iceberg for the whole story of what influences Nb_3Sn composition. Next, we can use this model to guide the design and processing of Nb_3Sn conductors in order to improve the Sn content and reduce the gradient. However, in order to do that, we still need to know how each design or processing factor influences these fundamental parameters in Eq. (4). In certain cases, one factor may influence more than one of these parameters (e.g., a higher heat treatment temperature leads simultaneously to larger k_I, k_{II}, larger d, larger D, and larger X_s – because it enhances μ_{Sn} of the Sn source); in such a case, we need to know the variation of each parameter with this factor. Overall, this model sets up a framework for compound composition calculation that bridges the material design/processing and structure (chemistry).

Next, in order to investigate the influence of the diffusion rate versus reaction rate, let us look at the new internally-oxidized Nb_3Sn, which displays some features distinct from conventional Nb_3Sn. One of the features is particularly interesting for this theory: we have previously noted that internally-oxidized Nb_3Sn has noticeably lower layer growth rate than conventional, non-oxidation Nb_3Sn for reaction temperatures below 750°C [13]. Here we want to point out that in addition to allowing a calculation of the compound composition, the above model can also be used to calculate the compound layer growth rate, because $\mathrm{d}l/\mathrm{d}t = J_{II}V_m/X_f$. After inserting Eqs. (2) and (4), we obtain a second-order differential equation regarding $l(t)$. While obtaining its general solution is beyond the scope of this article as we are focused on the composition, a few simple conclusions can be drawn from the model: (1) as $D_{eff}/l >> k_{II}$ (i.e., reaction-rate limited), $l = [k_I \cdot k_{II} \cdot V_m \cdot (X_s - 0.17)/(k_I \cdot X_s + 0.17k_{II})] \cdot t$; (2) for $k_{II} >> D_{eff}/l$ (i.e., diffusion rate limited), $l = [2V_m \cdot D_{eff} \cdot (X_s - 0.17)/0.17]^{0.5} \cdot t^{0.5}$; (3) in a general case between the two extremes, the layer growth rate depends on k_I, k_{II}, D_{eff}, and X_s, all having positive influence; (4) from the above two extreme cases and a general case in between, we see that higher X_s (i.e., higher μ_{Sn} of the Sn source) always leads to higher Nb_3Sn layer growth rate – this has been demonstrated in a number of experiments [10,19]. For example, using Cu-Sn source with certain alloying elements (e.g., Zn [23]) that can increase the μ_{Sn} of the Cu-Sn alloys has been demonstrated effective to enhance the Nb_3Sn layer growth rate [23].

The influence of internal oxidation on the Nb_3Sn layer growth rate in a general case indicates that it must change at least one of the four parameters (k_I, k_{II}, D_{eff}, and X_s). Next, let us investigate the possible influence of internal oxidation on each parameter so that we can use Eq. (4) to predict its influence on the Sn content. First of all, we expect that the internal

oxidation has little influence on the μ_{Sn} of the Sn source (as O is absorbed by the Nb-Zr alloy and does not reside in Nb_6Sn_5 or Cu-Sn alloys) or on the reaction rate constant at the Sn source/Nb_3Sn interface because of similar chemistry at this interface to that in non-oxidized Nb_3Sn wires. However, the internal oxidation may have an influence on the diffusion rate. It is well known that internally-oxidized Nb_3Sn has dramatically smaller grain size than non-oxidized Nb_3Sn (reduction by two times or more [13,14]), and our APT analysis shows that their grain boundary widths are similar (~2 nm in terms of segregation region [20]). These observations seem to suggest that internal oxidation may enhance the diffusion rate due to smaller grain size; however, we are not sure about the change of the grain boundary diffusivity, as $D_{eff} = D/V_m \cdot (2w/d)$. On the other hand, we expect that the internal oxidation may suppress the reaction rate at the Nb_3Sn/Nb interface. From the APT results in Figs. 2c and 2d we see high concentrations of Zr and O atoms at the Nb_3Sn/Nb interface, and it is very likely that they slow down the migration of the interface with a "solute drag effect" [24], which accounts for the reduced Nb_3Sn layer growth rate. According to Eq. (4), the reduced k_{II} should lead to increased Sn content in the Nb_3Sn layer. So, let us compare the measurement results of internally-oxidized and control Nb_3Sn to see if this is in fact true.

3. Experimental results and discussions

For the purpose of our Sn content study, an internal oxidation wire based on a 48/61-filament design (i.e., 13 Cu + 48 Nb_3Sn filaments) with a diameter of 0.84 mm and a Cu/non-Cu area ratio of 1.3 was used, and is named IO61 here. Its filament was fabricated by filling a mixture of Cu, Sn, and SnO_2 powders into a Nb-1at.%Zr-4at.%Ta tube. Other details and SEM images of this wire can be found in [14]. In addition to the three basic elements (Nb, Sn, Cu) necessary for Nb_3Sn formation, this wire has three additional elements (Ta, Zr, O) with two distinct functions: Ta is a dopant that dissolves in Nb_3Sn lattice to improve Nb_3Sn B_{c2}, while Zr and O are for the internal oxidation process (i.e., O supplied by the SnO_2 powder diffuses into the Nb-Zr-Ta tube during the early stages of the reaction and selectively oxidizes Zr to form ZrO_2 particles in Nb_3Sn). In order to have a rigorous comparison with IO61, we fabricated several reference wires with the same design as the IO61, each lacking only one element in turn: (1) a wire without Ta (named here "Ref-noTa") was made using similar Cu+Sn+SnO_2 powders and a Nb-1at.%Zr tube, (2) a wire without Zr (named "Ref-noZr") was made using similar Cu+Sn+SnO_2 powders and a Nb-4at.%Ta tube, (3) a wire without O (named "Ref-noO") was made using the same Nb-1at.%Zr-4at.%Ta tube but with only Cu+Sn powders (i.e., no SnO_2 powder). The Cu/Sn ratios of these wires were all similar. In addition, a state-of-the-art powder-in-tube (PIT) wire made by Bruker, which uses a Nb-4at.%Ta tube but no Zr or O, was also used as a reference wire (named here "PIT-Bruker"). It has 192/217 filaments and a 0.78 mm diameter, with other detailed information given in [14]. All the wires were heat treated under vacuum at the same 675°C, with the reaction times for the IO61, Ref-noTa, Ref-noZr, Ref-noO, and PIT-Bruker wires being 380, 300, 200, 120, and 50 hours, respectively. The reaction durations were chosen to drive them to complete reaction; the PIT-Bruker had shorter reaction time because its filament size (~40 μm) is smaller than that of others (~84 μm). Fig. 4a gives the Sn contents of the Nb_3Sn layers of the above five wires measured using energy dispersive spectroscopy (EDS) attached with a SEM. For the EDS measurements, 25 kV voltage was used,

with a collection rate above 40000 counts per second, and data were collected for 30 seconds for each spot. The interaction volume of each EDS spot was ~1 μm in diameter. The spots spanned the Nb_3Sn layer formed by diffusion reaction (which is also called the "fine-grain" Nb_3Sn layer by some papers [21]), with the Spot #1 closest to the Sn source, and Spot #7 closest to the Nb_3Sn/Nb interface. For each wire, measurements were made on three filaments and averaged. The error bars in Fig. 4a reflect both the statistical and systematic errors.

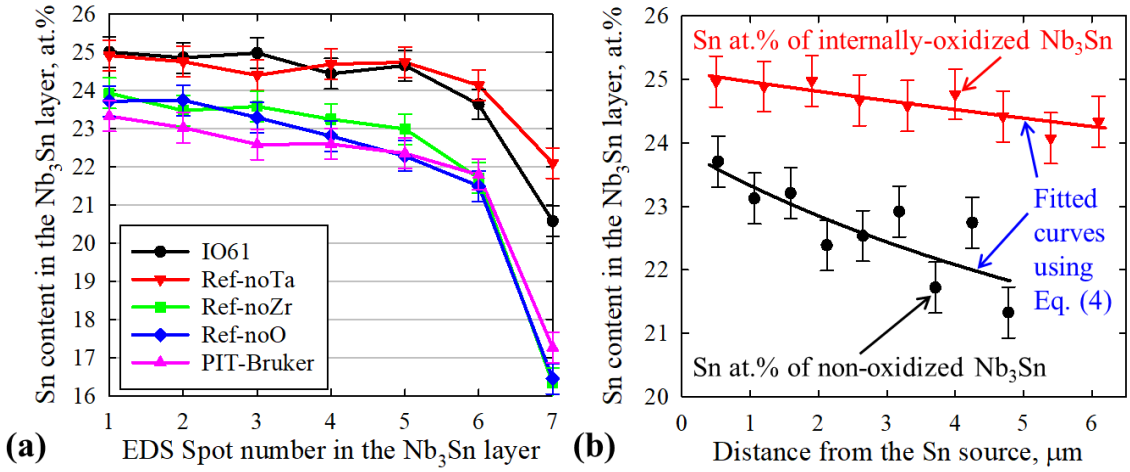

Fig. 4. (a) EDS-measured Sn contents in the Nb_3Sn layers of different samples (note that the Spot #7 in each sample, i.e., the one closest to the Nb_3Sn/Nb interface, may partially sample the Nb region), and (b) fittings using Eq. (4) to an internally-oxidized sample and a non-oxidized sample, both having only Nb_6Sn_5 as the Sn source.

Because the EDS analysis of Spot #7 may be partially sampling Nb regions due to the interaction volume of the electron beam, below we mainly discuss the Sn content results of Spot #1 through Spot #6. From Fig. 4a it can be seen that within the measurement error range the five wires fall into two groups: (1) Ref-noZr, Ref-noO, and PIT-Bruker generally had Sn contents between 21.5 and 24 at.%, which is typical for conventional Nb_3Sn wires [5,9,10,18]; (2) the other group, including IO61 and Ref-noTa, had Sn concentrations between 24 and 25 at.%, close to stoichiometry. The latter group of wires are those with internal oxidation (with and without Ta dopant), while the former group of wires are those without internal oxidation due to lack of either Zr or O. By comparing these wires, we can clearly see that the internal oxidation indeed significantly improves the Sn content of Nb_3Sn (by at least 1 at.%) for the majority of a Nb_3Sn layer (the last-formed part still has low Sn contents as in non-oxidized wires, due to low X_s). Since the samples shown in Fig. 4a were fully reacted and had Cu-Sn alloys as the Sn source as well, we cannot fit the data using Eq. (4) due to changing X_s. In order to understand how the internal oxidation influences the parameters in Eq. (4), we measured the Sn content of IO61 reacted at 650°C for 200 hours so that it only had Nb_6Sn_5 as the Sn source, and let us compare its fitted parameters with those of the non-oxidized wire reacted at 650°C for 48 hours shown in Fig. 3a. The obtained fitted parameters for the internally-oxidized Nb_3Sn in Fig. 4b are that: $k_{II}/k_I = 0.047$, and $k_{II}/D_{eff} = 0.02$/m. Comparing these parameters with those of the non-oxidized sample, it can be seen that the major effect of internal oxidation is on k_{II}: the significant suppress on the reaction rate at the Nb_3Sn/Nb interface leads to substantial

decreases in both k_{II}/k_I and k_{II}/D_{eff}, which further leads to significant increase of the Sn content in the Nb_3Sn layer, as well as a reduced Nb_3Sn layer growth rate.

Next let us compare the B_{c2} of our internal oxidation wires with present state-of-the-art Nb_3Sn wires to see if the higher Sn content can lead to superior high-field performance. Two common ways to measure B_{c2} are: (1) directly measuring electrical resistance vs magnetic field (*R*-*B*), and (2) measuring critical current density J_c at each field and extracting B_{c2} from the J_c-*B* curve. J_c is a property that directly determines the application of a superconductor in magnets, and B_{c2} has a critical influence on J_c because J_c decreases with *B*, vanishing at B_{c2}. Therefore, we performed two types of transport tests: (1) resistance vs field (*R*-*B*) measurements using a sensing current of 0.1 A, and (2) voltage vs current (*V*-*I*) measurements at various magnetic fields, allowing determination of J_c-*B* curves. All tests were at 4.2 K in a 31 T magnet at the National High Magnetic Field Laboratory (NHMFL), with fields perpendicular to wire axes. Great care was taken to ensure that each sample was centered within the magnet. The *R*-*B* tests were performed on samples 15 mm in length with a voltage tap spacing of 5 mm. The *V*-*I* measurements were performed on straight samples 35 mm in length with a voltage tap separation of 6 mm. A criterion of 0.1 μV/cm was used to determine the J_c values.

Our focus was to compare the properties of our internal oxidation wires with present state-of-the-art Nb_3Sn to see if we could push the Nb_3Sn performance to a new level. In addition to the IO61 wire used above, we also measured another internal oxidation wire we fabricated recently, which had a similar filament recipe with IO61 but 180/217 filaments, 0.98 mm diameter, and a Cu/non-Cu ratio of 1.15, named here IO217. SEM images of IO217 after 685°C/120h are shown in Figs. 1b and 1c. For the state-of-the-art Nb_3Sn wires, besides the PIT-Bruker wire, a "rod-restack-process" (RRP®) wire is also used here as a reference, with its detailed information given in [14]. Both were heat treated with their recommended schedules [14]. The *R*-*B* curves of the four wires are shown in Fig. 5a. At low fields they were superconducting, and then with increasing field eventually experienced a transition to the normal state. Below we take the fields at 10% and 99% of the full resistance as $B_{c2\text{-}10\%}$ and $B_{c2\text{-}99\%}$, respectively. The width of the transition reflects the uniformity of a superconductor. The 4.2 K $B_{c2\text{-}10\%}$ and $B_{c2\text{-}99\%}$ of the RRP® wire were ~25 and ~26.2 T, respectively, which are typical for RRP® wires reacted at 665°C [10]. The PIT-Bruker wire had 4.2 K $B_{c2\text{-}10\%}$ and $B_{c2\text{-}99\%}$ of 26 and 27.1 T, respectively, which are similar to what Godeke obtained for PIT wires reacted at 675°C [5] and are ~1 T higher than those of the RRP® wire. The fact that PIT wires have higher B_{c2} than RRP® wires is well-known, and can be explained by their different Sn sources based on our model. The 4.2 K $B_{c2\text{-}10\%}$ and $B_{c2\text{-}99\%}$ of IO61 were 27 and 28.1 T, respectively, ~1 T higher than those of the PIT-Bruker wire. The IO217 sample had even higher 4.2 K $B_{c2\text{-}10\%}$ and $B_{c2\text{-}99\%}$: 27.1 and 28.2 T, respectively.

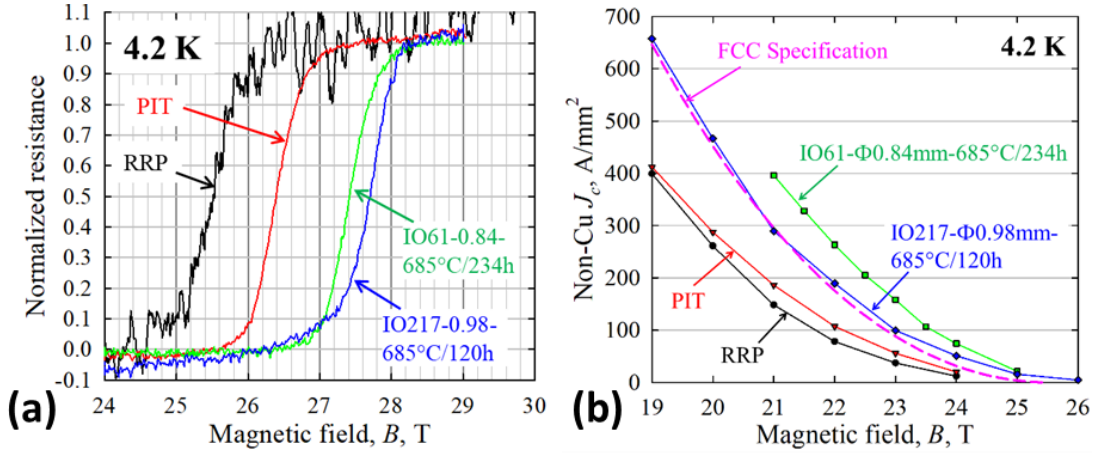

Fig. 5. The measured (a) *R*-*B* and (b) non-Cu J_c-*B* curves of the reference wires and the internal oxidation wires at 4.2 K.

The measured non-Cu J_c-*B* curves of the above four wires are shown in Fig. 5b, along with the FCC J_c specification [6]. Fittings were made to their J_c-*B* data with a commonly-used model [25], giving extrapolated B_{c2} values (at 4.2 K) of 24.7, 25.5, 26.3, and 26.6 T for the RRP®, PIT-Bruker, IO61, and IO217 wires, respectively. A summary of the B_{c2} values obtained from the two methods is shown in Table 1. The B_{c2} values from the two methods are somewhat different due to sample non-uniformity and different criteria used, but both show that the internal oxidation wires have noticeably higher B_{c2} than present state-of-the-art wires (~2 T higher than RRP® and ~1 T higher than PIT-Bruker). These results indicate that the internally-oxidized Nb_3Sn indeed has higher B_{c2}, which is most likely due to their higher Sn contents. . In fact, to the best of our knowledge, 28.2 T is the highest measured B_{c2}(4.2 K) value reported in Nb_3Sn multi-filamentary wires ever. On the other hand, our measurements showed that the internally-oxidized samples did not have noticeably higher T_c than the PIT-Bruker wire. The variations of B_{c2} and T_c with Sn content for Ta-doped Nb_3Sn, which have not been well studied, are needed to explain the B_{c2} and T_c changes in internally-oxidized Nb_3Sn. Other possibilities include that there might be extra O dissolving in Nb_3Sn, or the intragranular ZrO_2 nanoparticles cause distortion of Nb_3Sn lattice, both increasing normal-state resistivity of Nb_3Sn, which may enhance B_{c2} but reduce T_c [8].

Table 1
Summary of the measured B_{c2} values (4.2 K) of state-of-the-art Nb_3Sn and internal oxidation Nb_3Sn wires

B_{c2}(4.2 K)	RRP®	PIT-Bruker	IO61	IO217
B_{c2} determined from J_c-*B* curves	24.7	25.5	26.3	26.6
$B_{c2\text{-}10\%}$ from *R*-*B* curves	25	26	27	27.1
$B_{c2\text{-}99\%}$ from *R*-*B* curves	26.2	27.1	28.1	28.2

High B_{c2} is important for applications of Nb_3Sn superconductors at high fields. From Fig. 5b we see that B_{c2} has a significant influence on J_c, and the higher the field is, the stronger the influence becomes, due to proximity to B_{c2}. For example, the non-Cu J_c value of IO217 is 1.65

times of that of the RRP® wire at 19 T, but becomes 2 times of the latter at 21 T, and 2.7 times at 23 T. Of course, this is partially contributed by a pinning force peak field shift effect in internally-oxidized Nb_3Sn [14], but higher B_{c2} also plays an important role. This is important because Nb_3Sn superconductor is used for building nuclear magnetic resonance (NMR) magnets at 23 T operating at 1.9 K (operation at 4.2 K is prevented by the insufficient J_c and B_{c2} at 4.2 K). Here it is worth noting that although IO217 has lower non-Cu J_c than IO61 due to lower filament quality (e.g., reaction extent and uniformity) as a result of smaller filament size (50 μm vs 84 μm), IO217 already has non-Cu J_c above the challenging FCC specification above 19 T. Further wire development is expected to improve quality and thus J_c of internal oxidation wires with 217 filaments.

Finally, it is worth discussing the general applicability of our model, developed using Nb_3Sn as an example, to other non-stoichiometric compounds formed by diffusion reaction processes with low bulk diffusivities. If a non-stoichiometric compound has a sufficiently low bulk diffusivity such that the bulk diffusion distance is small with respect to the grain boundary width [26] (as Nb_3Sn does), then the bulk diffusion can be regarded as small enough to be neglected. In this case, the model, with certain parameters modified, can be applied to that compound, and the qualitative conclusions still apply: i.e., what determines the composition profile of a single compound layer includes the chemical potential of the diffusing species in its source, the ratios of the reaction rates at the two interfaces, and the competition between the diffusion rate and the reaction rates. On the other hand, there are also systems with bulk diffusivities that are low but perhaps not low enough to allow us to totally neglect the presence of bulk diffusion. In this case, the bulk composition profile is not totally persistent, but changes slowly with annealing, perhaps preventing itself from reaching the equilibrium compositions within a realistic annealing time. For such compounds, the model presented in this paper represents an extreme case that can be used for the evaluation of their composition profiles. To determine the accurate composition at a specific time, a treatment for the homogenization between the lattice and the grain boundaries for each grain (e.g., leakage of the diffusing species from the grain boundaries to the adjacent bulk if the latter has a lower chemical potential) must be added on top of the present model, which is beyond the scope of this work.

4. Conclusions

This paper explores what determines the composition of a non-stoichiometric compound formed in a diffusion reaction process, and shows that the bulk diffusivity has a critical influence. If the bulk diffusivity is very low, the composition profile of the compound layer is just an accumulation of local “snapshots” of the composition of each frontier layer before it breaks away from the diffusion zone at the reactive interface, and the profile is persistent (i.e., it cannot be homogenized or reach equilibrium even with long annealing times). A model was developed to quantitatively determine the composition profile in this case, using the Nb_3Sn compound superconductor as an example, which shows that the composition profile is determined by (1) the chemical potential of the diffusing species in its source, (2) the ratios of the reaction rate constants for the two interfaces, and (3) the competition between the diffusion rate and the reaction rates, where the diffusion rate is determined by the grain boundary diffusivity, grain size, and grain boundary width. The model was then compared to the known

facts for Nb_3Sn compounds, and good agreement is seen. In particular, the importance of the competition between the diffusion rate and the reaction rates is seen in the emerging internal-oxidation-type Nb_3Sn wires. We show that, in agreement with Eq. (4), such wires have higher Sn contents than conventional, non-oxidized Nb_3Sn, and also higher B_{c2}, which significantly benefits the high-field performance. In general, this model provides a framework for us to understand how a design or processing parameter influences the composition of a non-stoichiometric compound with low bulk diffusivity and thus can be a tool for us to optimize the design and processing of such materials for composition control.

Declaration of interests

The authors declare that they have no known competing financial interests or personal relationships that could have appeared to influence the work reported in this paper.

CRediT authorship contribution statement

X. Xu: Conceptualization, Methodology, Formal analysis, Investigation, Writing - original draft. **M. Sumption:** Investigation, Writing - review & editing. **J. Lee:** Investigation. **J. Rochester:** Investigation. **X. Peng:** Investigation, Funding acquisition.

Acknowledgements

This work was supported by the LDRD program of Fermilab, the Early Career Research Program as well as Hyper Tech SBIR DE-SC0013849 and DE-SC0017755 by US Department of Energy. The authors want to thank Ian Pong from LBNL for supplying the RRP® and standard PIT wires that were used as references in this work. Some tests were performed at the NHMFL, which is supported by NSF Cooperative Agreement No. DMR-1644779 and the State of Florida. The tests at the NHMFL were greatly helped by Jan Jaroszynski and Griffin Bradford. The authors are grateful to the Applied Superconductivity Center (ASC) of Florida State University (FSU) for letting us use the critical current test system, and for the independent verification tests of J_c for the RRP® and IO61 samples. Atom-probe tomography was performed at the Northwestern University Center for Atom-Probe Tomography (NUCAPT). The LEAP tomograph at NUCAPT was purchased and upgraded with grants from the NSF-MRI (DMR-0420532) and ONR-DURIP (N00014-0400798, N00014-0610539, N00014-0910781, N00014-1712870) programs. NUCAPT received support from the MRSEC program (NSF DMR-1720139) at the Materials Research Center, the SHyNE Resource (NSF ECCS-1542205), and the Initiative for Sustainability and Energy (ISEN) at Northwestern University.

Appendix

The reaction rate at the Nb_3Sn/Nb interface, expressed in terms of the Sn flux from the frontier layer to the Nb region (in mol/m^2-s), is $J_r = r[1-\exp(-\Delta\mu/RT)]$, where r (in mol/m^2-s) is a rate constant for this process which depends on temperature (T) and an energy barrier (following an Arrhenius-type equation), R is the gas constant, and $\Delta\mu = \mu_{Sn}$(Nb-X_fSn) − μ_{Sn}(Nb-

17%Sn) is the μ_{Sn} drop and thus the driving force for transfer of Sn atoms. Here we notice that $\exp\{-[\mu_{Sn}(\text{Nb-}X_f\text{Sn}) - \mu_{Sn}(\text{Nb-17\%Sn})]/RT\} = a_{Sn}(\text{Nb-17\%Sn})/a_{Sn}(\text{Nb-}X_f\text{Sn})$, where a_{Sn} is the activity of Sn in Nb_3Sn and is a monotonically increasing function of Sn content. Because Nb_3Sn has a narrow composition range, if we perform a Taylor series expansion for $1- a_{Sn}(\text{Nb-17\%Sn})/a_{Sn}(\text{Nb-}X_f\text{Sn})$ (i.e., the whole term being treated as a function, with X_f being the variable) around Sn content of 17% and neglect high-rank terms, we find that it can be reduced to a simple form of $c\cdot(X_f-17\%)$, where c is a unitless constant related to a_{Sn} and its derivative for the Sn content of 17%. If we define a reaction rate constant $k_{II} = r\cdot c$, the reaction rate at Interface II can be written in a very simple form: $J_{II} = k_{II}\cdot(X_f-17\%)$.

References

[1]. R.D. Noebe, R.R. Bowman, M.V. Nathal, Physical and mechanical properties of the B2 compound NiAl, Int. Mater. Rev. 38 (1993) 193-232.

[2]. M. Mudgel, V.P.S. Awana, G.L. Bhall, H. Kishan, Superconductivity of non-stoichiometric intermetallic compound NbB_2, Solid State Commun. 147 (2008) 439-442.

[3]. M. Friedricha, D. Teschnerb, A. Knop-Gerickeb, M. Armbrüster, Influence of bulk composition of the intermetallic compound ZnPd on surface composition and methanol steam reforming properties, J. Catal. 285 (2012) 41-47.

[4]. J.P. Charlesworth, I. MacPhail, P.E. Madsen, Experimental work on the niobium-tin constitution diagram and related studies, J. Mater. Sci. 5 (1970) 580-603.

[5]. A. Godeke, Performance boundaries in Nb_3Sn superconductors, Ph.D. dissertation, University of Twente, 2005.

[6]. A. Abada et al., FCC-hh: The Hadron Collider, Eur. Phys. J. Special Topics 228 (2019) 755–1107.

[7]. H. Devantay, J.L. Jorda, M. Decroux, J. Muller, R. Flükiger, The physical and structural properties of superconducting A15-type Nb-Sn alloys, J. Mat. Sci. 16 (1981) 2145-2153.

[8]. T.P. Orlando, J.A. Alexander, S.J. Bending, J. Kwo, S.J. Poon, R.H. Hammond, M.R. Beasley, E.J. McNiff, Jr., S. Foner, The role of disorder in maximizing the upper critical field in the Nb-Sn system, IEEE Trans. Magn. 17 (1981) 368-369.

[9]. T. Baumgartner, S. Pfeiffer, J. Bernardi, A. Ballarino, M. Eisterer, Performance limitations due to A-15 inhomogeneity in Nb_3Sn wires, Applied Superconductivity Conference (2018) 1MOr2B-02.

[10]. X. Xu, A review and prospects for Nb_3Sn superconductor development, Supercond. Sci. Technol. 30 (2017) 093001.

[11]. V.I. Dybkov, Solid State Reaction Kinetics, IPMS Publications, Kyiv, 2013.

[12]. X. Xu, M. Sumption, A model for the compositions of non-stoichiometric intermediate phases formed by diffusion reactions, and its application to Nb_3Sn superconductors, Sci. Rep. 6 (2016) 19096.

[13]. X. Xu, M.D. Sumption, X. Peng, Internally Oxidized Nb_3Sn Superconductor with Very Fine Grain Size and High Critical Current Density, Adv. Mater. 27 (2015) 1346-1350.

[14]. X. Xu, X. Peng, J. Lee, J. Rochester, M.D. Sumption, High Critical Current Density in Internally-oxidized Nb_3Sn Superconductors and its Origin, Scr. Mater. 186 (2020) 317-320.

[15]. G. Lefranc, A. Muller, Effect of Copper Additions to Superconducting Niobium-Tin Sinter Material, J. Less-Common Met. 45 (1976) 339-342.
[16]. M.J.R. Sandim, D. Tytko, A. Kostka, P. Choi, S. Awaji, K. Watanabe, D. Raabe, Grain boundary segregation in a bronze-route Nb_3Sn superconducting wire studied by atom probe tomography, Supercond. Sci. Technol. 26 (2013) 055008.
[17]. X. Xu, M.D. Sumption, X. Peng, unpublished results.
[18]. C.D. Hawes, P.J. Lee, D.C. Larbalestier, Measurements of the microstructural, microchemical and transition temperature gradients of A15 layers in a high-performance Nb_3Sn powder-in-tube superconducting strand, *Supercond. Sci. Technol.* 19 (2006) S27-37.
[19]. H. Müller, Th. Schneider, Heat treatment of Nb_3Sn conductors, Cryogenics 48 (2008) 323-330.
[20]. J. Lee, Z. Mao, X. Xu, D. Seidman, Unveiling the nucleation and growth of Zr oxide particles of internally-oxidized Nb_3Sn superconductors, to be submitted.
[21]. X. Xu, M.D. Sumption, E.W. Collings, A Model for Phase Evolution and Volume Expansion in Tube Type Nb_3Sn Conductors, Supercond. Sci. Technol. 26 (2013) 125006.
[22]. V. Abächerli, D. Uglietti, P. Lezza, B. Seeber, R. Flükiger, M. Cantoni, P.A. Buffat, The Influence of Ti Doping Methods on the High Field Performance of $(Nb,Ta,Ti)_3Sn$ Multifilamentary Wires Using Osprey Bronze, IEEE Trans. Appl. Supercon. 15 (2005) 3482-3485.
[23]. N. Banno, Y. Miyamoto, K. Tachikawa, Multifilamentary Nb_3Sn Wires Fabricated Through Internal Diffusion Process Using Brass Matrix, IEEE Trans. Appl. Supercon. 26 (2016) 6001504.
[24]. M. Hillert, B. Sundman, A treatment of the solute drag on moving grain boundaries and phase interfaces in binary alloys, Acta Metall., 24 (1976) 731-743.
[25]. T. Baumgartner, M. Eisterer, H.W. Weber, R. Flükiger, C. Scheuerlein, L. Bottura, Performance Boost in Industrial Multifilamentary Nb_3Sn Wires due to Radiation Induced Pinning Centers, Sci. Rep. 5 (2015) 10236.
[26]. D.E. Laughlin, K. Hono, Physical Metallurgy, fifth ed., Elsevier, Amsterdam, 2015.